ELSEVIER

Chemical Engineering Journal 139 (2008) 224–235

Chemical Engineering Journal

www.elsevier.com/locate/cej

Drag on ensembles of fluid spheres translating in a power-law liquid at moderate Reynolds numbers

N. Kishore [a], R.P. Chhabra [a,*], V. Eswaran [b]

[a] *Department of Chemical Engineering, Indian Institute of Technology, Kanpur 208016, India*
[b] *Department of Mechanical Engineering, Indian Institute of Technology, Kanpur 208016, India*

Received 12 June 2007; received in revised form 26 July 2007; accepted 27 July 2007

Abstract

This work elucidates the role of power-law rheology on the sedimentation velocity of an ensemble of mono-size spherical Newtonian droplets (free from surfactants) translating in a power-law continuous phase numerically by solving the momentum equations of both phases. A simple sphere-in-sphere cell model has been used to account for inter-drop interactions. In particular, in this study, the effects of the Reynolds number (Re_o), the internal to external fluid characteristic viscosity ratio (k), the volume fraction of the dispersed phase (Φ) and the power-law index of the continuous phase (n_o) on the external flow field, pressure drag (C_{dp}), friction drag (C_{df}) and total drag (C_d) coefficients have been analyzed over wide ranges of parameters as follows: $1 \leq Re_o \leq 200$, $0.1 \leq k \leq 50$, $0.2 \leq \Phi \leq 0.6$ and $0.6 \leq n_o \leq 1.6$. Based on the extensive numerical results obtained in this work, a simple predictive correlation has been proposed for the total drag coefficient, which can be used to predict the rate of sedimentation of ensembles of Newtonian fluid spheres in power-law liquids in a new application.

Keywords: Ensemble; Fluid sphere; Viscosity ratio; Power-law liquids; Drag; Viscous drop

1. Introduction

Due to their overwhelming applications in many chemical, biochemical and material processing industries, the motion of and mass transfer from drops in viscous liquids has received considerable attention in the literature. Typical applications include liquid–liquid extraction, liquid–liquid fluidization, bubble column reactors [1], sparged reactors, degassing of polymeric melts and glasses, production and stability of emulsions in paint, food processing [2], in personal care products and detergent industries, pipeline transport of oil/water emulsions, etc. [3,4]. In liquid–liquid contacting equipment, one fluid is often dispersed in the form of droplets in another immiscible fluid. For instance, the knowledge of the sedimentation velocity facilitates the sizing of contacting system if the desired residence time is known from other considerations, or conversely, for an existing system, it is used to calculate the mean contacting time. Similarly, the rate of sedimentation also helps in ascertaining the stability of an emulsion or the ease of separation by gravity depending upon an envisaged application. Therefore, the steady incompressible motion of an ensemble of liquid drops in another immiscible fluid medium represents an idealization of many industrially important applications. Hence, the sedimentation behaviour of ensembles of fluid spheres is a prerequisite for the understanding and designing of these transport processes. Therefore, the need to predict the rate of settling of liquid–liquid dispersion frequently arises in process engineering calculations. Experimental determination of the settling velocity of ensembles of drops is rather difficult due to the inherent difficulties. On the other hand, theoretical and/or numerical approach to the analysis of such systems can lead to useful methods to predict the rate of sedimentation of droplets while designing liquid–liquid contacting equipments. Consequently, over the years, considerable research efforts have been directed at developing reliable methods for the prediction of the rate of translation of single and ensembles of Newtonian droplets in an immiscible Newtonian media [5–7]. It is customary to express this information in terms of the usual Reynolds number, drag coefficient and the other pertinent dimensionless groups.

On the other hand, it is readily recognized that many high molecular weight polymers and their solutions, slurries, foams and emulsions encountered in several industrially important

* Corresponding author. Tel.: +91 512 2597393; fax: +91 512 2590104.
E-mail address: chhabra@iitk.ac.in (R.P. Chhabra).

1385-8947/$ – see front matter © 2007 Elsevier B.V. All rights reserved.
doi:10.1016/j.cej.2007.07.092

Nomenclature

C_d	total drag coefficient
C_{df}	friction drag coefficient
C_{dp}	pressure drag coefficient
dr	mesh size in r-direction
dt	time-step size
dθ	mesh size in θ-direction
k	internal to external fluid characteristic viscosity ratio
m	power-law consistency index (Pa s^n)
n	power-law flow behaviour index
p	pressure
QUICK	quadratic upstream interpolation of convective kinematics
r	radial distance
R	drop radius (m)
R_∞	cell boundary
Re	Reynolds number
SMAC	simplified marker and cell
U_o	settling velocity (m s^{-1})
v_r	r-component of velocity
v_θ	θ-component of velocity
v_ϕ	ϕ-component of velocity

Greek symbols

Φ	volume fraction of the dispersed phase
Π_ε	second invariant of the rate of strain tensor (s^{-2})
ε	rate of strain tensor (s^{-1})
ϕ	Azimuthal direction (°)
η	dynamic viscosity (Pa s)
λ	internal to external fluid density ratio, ρ_i/ρ_o
θ	streamwise direction (°)
ρ	density of fluid (kg m^{-3})
τ	shear stress (Pa)

Subscripts

i	Internal flow variable
o	External flow variable
r	r-component
ϕ	ϕ-component
θ	θ-component

applications display a range of non-Newtonian characteristics including shear-thinning, shear-thickening, yield stress and visco-elastic behaviour [8]. Despite their wide occurrence in diverse industrial applications, very little information is available on the sedimentation velocity of ensembles of drops in non-Newtonian fluids, especially beyond the creeping flow regime [4], though adequate information is available on the drag behaviour of a single bubble [9–13], a single solid particle [14,15] and a single drop [16–20] settling in quiescent power-law media. Similarly, some results are also available on the rise velocity of swarms of spherical bubbles [21–25] in power-law fluids encompassing the creeping and potential flow regimes with limited results in the intermediate Reynolds number region. Therefore, this work is concerned with the numerical investigation of the drag behaviour of ensembles of mono-size Newtonian spherical droplets sedimenting in power-law liquids at moderate Reynolds numbers. It is, however, appropriate to start with a short review of the scant literature available in this field.

2. Previous work

In order to describe the relative motion between ensembles of drops and a continuous phase, in addition to the usual conservation laws, one needs to have a mathematical description of the inter-drop hydrodynamic interactions. Broadly, there are two approaches available in the literature to describe the inter-drop hydrodynamic interactions. In the first approach, the governing field equations are solved for a specific configuration of drops (such as triangular, simple cubic, body centred cubic, face centred cubic, periodic arrays, etc.). Although, this approach is rigorous, extrapolation of results even to a slightly different configuration is generally not possible [4]. These results are frequently expressed in the form of a correction factor to be applied to the case of a single droplet and the correction factor is a strong function of the concentration of the dispersed phase, and the type of packing of droplets enters via the corresponding maximum packing fraction. As far as known to us, this approach has not been extended to finite Reynolds number situations even for Newtonian fluids, let alone to non-Newtonian liquids. In the second approach, somewhat less rigorous, inter-drop hydrodynamic interactions are approximated by postulating the each fluid sphere to be surrounded by a hypothetical concentric envelope of the continuous phase. The size of this cell is chosen such that the volume fraction of the dispersed phase in each cell is equal to the overall mean volume fraction of the dispersed phase in the ensemble. This approach is equivalent to imposing a wall effect on a single particle. Thus, Happel [26] proposed the cell boundary to be frictionless thereby emphasizing the non-interacting nature of cells. On the other hand, Kuwabara [27] advocated the use of the zero vorticity condition at the cell boundary. While this approach has been quite successful in a range of settings, it is also open to criticism especially in terms of the boundary condition prescribed on the cell boundary. While it is virtually impossible to offer a sound theoretical justification for either of these boundary conditions, suffice it to say here that owing to the extra dissipation in the zero vorticity cell model, the resulting values of the drag coefficients are larger than those obtained by using the free surface cell model [4], though both models have been used extensively in the literature to model transport processes in concentrated multi-particle systems and currently available experimental results are not able to discern between these two models.

The free surface cell model has been extensively used to study the Newtonian and other generalized Newtonian fluids flow through clusters of bubbles, drops and solid particles. Thus, for instance, using this approach, approximate upper/lower bounds and numerical results on drag coefficients for swarms of spherical bubbles rising in Newtonian and in generalized Newtonian fluids including power-law fluids, Carreau model

fluids [18,21–25,28,29] are now available in the literature. Thus, combined together, the currently available results on bubble swarms in power-law fluids encompass the creeping and potential flow regimes, with limited results being available in between these two limits. Lee et al. [30] have employed these two cell models to contrast the analytical and numerical results of convective mass transfer rates of swarms of circulating bubbles in a Newtonian medium for moderate concentrations of bubbles in the swarm. Similarly, there are a few studies related to the flow and mass/heat transfer in Newtonian and other generalized Newtonian fluids in fixed and fluidized beds of solid spheres using both these cell models [31–34]. Detailed examination of these results shows a good match with the conventional capillary models, especially at high values of voidage [35,36]. Other applications of this approach include the electrophoresis of a concentrated spherical dispersion in a Carreau fluid under the conditions of low electric potential and weak externally applied electric field [37,38].

In contrast, very little information is available on the sedimentation of ensembles of drops translating even in Newtonian liquids, let alone in non-Newtonian continuous phase. Gal-Or and Waslo [39] were the first to use the free surface cell model to study the creeping motion of ensembles of mono-size drops in another immiscible Newtonian liquid with and without the presence of surfactants. Subsequently, this approach has been extended to predict the drag on ensembles of drops moving slowly (creeping region) in power-law and other generalized Newtonian fluids [40–44]. Tripathi and Chhabra [45] extended the study of Gal-Or and Waslo [39] to the case when both phases obey power-law fluid behaviour. This model has also been used successfully to capture the sedimentation behaviour of two-fluid spheres [46] and of composite spheres [47] in the creeping flow regime. Recently, Jung and Lee [48] analytically studied the flow field in ensembles of fluid spheres in low Knudsen regime using these two cell models. Subsequently, they have evaluated a general solution for the flow field around ensembles of fluid spheres in the low Knudsen number regime. Beyond the creeping flow conditions, only Kishore et al. [7] have numerically solved the complete Navier–Stokes equations for both (Newtonian) phases simultaneously up to moderate Reynolds numbers of 500.

The aforementioned range of applications shows the extremely versatile nature of this simple approach. Therefore, the free surface cell model has been used in this work to examine the role of power-law rheology of the continuous phase on the sedimentation of an ensemble of mono-size Newtonian drops in a quiescent power-law liquid. In particular, extensive numerical results are reported for wide ranges of the pertinent dimensionless parameters.

3. Problem statement and description

Consider an ensemble of mono-size and clean Newtonian spherical droplets of radius R translating steadily in a quiescent power-law liquid as shown schematically in Fig. 1(a). Both (continuous and dispersed) phases are assumed to be incompressible. The surface tension is assumed to be large (i.e., Weber number is very small) so that the drops retain their spherical

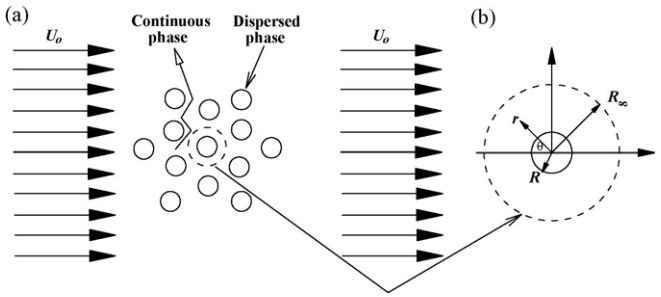

Fig. 1. (a) Schematic representation of the flow and (b) the cell model idealization.

shape under all conditions encompassed in this investigation. Based on the currently available experimental information, it is known that for Newtonian systems, considerable droplet oscillations or deviations from the spherical shape occur beyond a critical value of Weber number of approximately 4. This value corresponds to the Reynolds number in the range of 300–1000 depending upon the system properties. Though no analogous information is available for droplets in power-law liquids, the scant analytical and experimental results seem to suggest that the visco-elasticity causes much greater shape distortions than the shear-dependent viscosity of the continuous phase [4]. In view of this, the aforementioned criterion is assumed to apply in the present case also, at least as a first approximation. Within the framework of the free surface cell model, the inter-drop hydrodynamic interactions are approximated by postulating each drop to be surrounded by a hypothetical envelope of continuous fluid of radius R_∞ as shown in Fig. 1(b). The size of the envelope is chosen such that the volume fraction of the dispersed phase of each cell is equal to the overall mean volume fraction of the dispersed phase in the system. Qualitatively, this approach hinges on the fact that the increased drag on a single drop in an ensemble due to the hydrodynamic interactions with the neighbouring drops can be approximated by imposing an equivalent wall effect. This approach converts a difficult many body problem into a conceptually simpler one body equivalent by indirectly accounting for inter-drop interactions, in terms of drop hold-up which is function of the outer domain radius (R_∞). It is also appropriate to add here that while in real systems wake interactions occur which can lead to distorted shapes and lift forces, especially in concentrated systems. While these effects can give rise to a chaotic behaviour and produce complex flow field, but the overall drag is believed to be influenced mainly by the concentration of the dispersed phase.

A spherical coordinate system (r, θ, ϕ) with its origin located at the centre of the drop is employed here, polar axis ($\theta = 0$) is directed along the direction of flow as shown in Fig. 1(b). The flow is two-dimensional, thus, $v_\phi = 0$ and no flow variable depends upon the ϕ-coordinate. The dimensionless governing equations (in their conservative form) for this flow, in both phases, can be written as follows:

- Continuity equation

$$\frac{1}{r^2}\frac{\partial}{\partial r}[r^2(v_r)_{\mathrm{i,o}}] + \frac{1}{r\,\sin\theta}\frac{\partial}{\partial\theta}[(v_\theta)_{\mathrm{i,o}}\,\sin\theta] = 0 \qquad (1)$$

- r-Component of momentum equation

$$\frac{\partial(v_r)_{i,o}}{\partial t}+\frac{1}{r^2}\frac{\partial}{\partial r}\left[r^2(v_r)_{i,o}^2\right]+\frac{1}{r\sin\theta}\frac{\partial}{\partial\theta}[(v_r)_{i,o}(v_\theta)_{i,o}\sin\theta]-\frac{(v_\theta)_{i,o}^2}{r}=-\frac{\partial p_{i,o}}{\partial r}+\frac{2^{(n_{i,o}+1)}}{Re_{i,o}}\left[(\varepsilon_{rr})_{i,o}\frac{\partial\eta_{i,o}}{\partial r}+\frac{(\varepsilon_{r\theta})_{i,o}}{r}\frac{\partial\eta_{i,o}}{\partial\theta}\right]+\frac{2^{n_{i,o}}\eta_{i,o}}{Re_{i,o}}\left[\frac{1}{r^2}\frac{\partial^2}{\partial r^2}(r^2(v_r)_{i,o})+\frac{1}{r^2\sin\theta}\frac{\partial}{\partial\theta}\left(\sin\theta\frac{\partial(v_r)_{i,o}}{\partial\theta}\right)\right] \tag{2a}$$

- θ-Component of momentum equation

$$\frac{\partial(v_\theta)_{i,o}}{\partial t}+\frac{1}{r^2}\frac{\partial}{\partial r}[r^2(v_r)_{i,o}(v_\theta)_{i,o}]+\frac{1}{r\sin\theta}\frac{\partial}{\partial\theta}\left[(v_\theta)_{i,o}^2\sin\theta\right]+\frac{(v_r)_{i,o}(v_\theta)_{i,o}}{r}=-\frac{1}{r}\frac{\partial p_{i,o}}{\partial\theta}+\frac{2^{(n_{i,o}+1)}}{Re_{i,o}}\left[(\varepsilon_{r\theta})_{i,o}\frac{\partial\eta_{i,o}}{\partial r}+\frac{(\varepsilon_{\theta\theta})_{i,o}}{r}\frac{\partial\eta_{i,o}}{\partial\theta}\right]+\frac{2^{n_{i,o}}\eta_{i,o}}{Re_{i,o}}\left[\frac{1}{r^2}\frac{\partial}{\partial r}\left(r^2\frac{\partial(v_\theta)_{i,o}}{\partial r}\right)+\frac{1}{r^2}\frac{\partial}{\partial\theta}\left(\frac{1}{\sin\theta}\frac{\partial}{\partial\theta}[(v_\theta)_{i,o}\sin\theta]\right)+\frac{2}{r^2}\frac{\partial(v_r)_{i,o}}{\partial\theta}\right] \tag{2b}$$

where subscripts i, o denote the internal (dispersed) and external (continuous) flow variables, respectively.

For an incompressible fluid, the extra stress tensor is related to the rate of the strain tensor as [49]:

$$\tau_{xy}=2\eta\varepsilon_{xy};\quad x,y=r,\theta,\phi \tag{3}$$

and the viscosity of a power-law liquid is given by:

$$\eta=\left(\frac{\prod_\varepsilon}{2}\right)^{(n-1)/2} \tag{4}$$

where Π_ε is the second invariant of the rate of deformation tensor and its expression in terms of v_r, v_θ, v_ϕ and their derivatives is available in standard books (e.g., see Ref. [49]).

In Eqs. (1)–(4), the velocity terms have been scaled using U_o, radial coordinate r using the drop radius R, pressure using (ρU_o^2), components of the rate of strain tensor by (U_o/R), viscosity by a reference viscosity η_{ref}, shear stress by $\eta_{ref}(U_o/R)$ and time by (R/U_o). Here η_{ref} is defined as $\eta_{ref}=m(U_o/R)^{(n-1)}$, where m is the power-law fluid consistency index and n is the power-law behaviour index.

The Reynolds number is defined as follows:

$$Re_o=\frac{\rho_o U_o^{(2-n_o)}(2R)^{n_o}}{m_o} \tag{5}$$

Obviously, the two Reynolds numbers, Re_i and Re_o are interrelated via the characteristic viscosity ratio and density ratio as follows:

$$Re_i=\frac{Re_o\lambda}{k} \tag{6}$$

where, ρ is the density of fluid, λ is the density ratio $(=\rho_i/\rho_o)$ and k is the characteristic viscosity ratio defined as:

$$k=\left(\frac{\eta_i}{m_o}\right)\left(\frac{2R}{U_o}\right)^{(n_o-1)} \tag{7}$$

Although our main interest here is to obtain the steady state solution, the transient terms are retained in Eqs. (2a) and (2b) as the false-transient scheme has been used to solve these equations.

As noted earlier, the radius of the outer spherical envelope can be related to the overall mean volume fraction of the dispersed phase, Φ, as:

$$R_\infty=\Phi^{-1/3} \tag{8}$$

Therefore, by simply varying the value of R_∞, one can simulate the ensembles of various volume fractions of the dispersed phase including the limiting case of a single droplet by setting $R_\infty\to\infty$, i.e., $\Phi\to 0$. Conversely, one can readily calculate the value of R_∞ for known values of the volume fraction of the dispersed phase and the droplet size.

The dimensionless boundary conditions for this flow configuration within the framework of the free surface cell model can be written as follows:

- At the cell boundary ($r=R_\infty$):

$$(v_r)_o=-\cos\theta \tag{9a}$$

$$(\tau_{r\theta})_o=0 \tag{9b}$$

- At the liquid–liquid interface ($r=1$):

$$(v_r)_i=(v_r)_o=0 \tag{10a}$$

$$(v_\theta)_i=(v_\theta)_o \tag{10b}$$

$$(\tau_{r\theta})_i=(\tau_{r\theta})_o \tag{10c}$$

- Along the axis of symmetry ($\theta=0,\pi$):

$$(v_\theta)_i=0;\qquad \frac{\partial(v_r)_i}{\partial\theta}=0 \tag{11a}$$

$$(v_\theta)_o=0;\qquad \frac{\partial(v_r)_o}{\partial\theta}=0 \tag{11b}$$

- At the centre of the fluid sphere ($r=0$):

$$(v_r)_i \text{ and } (v_\theta)_i \text{ remain finite} \tag{12}$$

Due to the zero shear stress condition, the cell boundary is frictionless thereby emphasizing the non-interacting nature of the cells [4,26]. All other boundary conditions used herein are fairly standard, e.g., see Refs. [4–6], but are briefly elaborated here. Eqs. (10a)–(10c) imply the zero radial mass flux, the continuity of the tangential velocity and of the shear stress, respectively, at the surface of the drop. Eqs. (11a) and (11b) arise from the symmetry considerations of the flow in the range of conditions, mainly the Reynolds number. This justifies the solution of the equations to be obtained only in half of the domain, as the pressure and velocity fields in the upper and lower halves of the drop for $Re_o\le 200$ are simply the mirror image of each other. Finally Eq. (12) simply ensures that the velocity components at

the centre of the drop are bounded and finite. Eqs. (1), (2a) and (2b), subject to the boundary conditions outlined in Eqs. (9)–(12) provide the theoretical framework to map the flow domain, i.e., $0 \le r \le 1$, $1 \le r \le R_\infty$ and $0 \le \theta \le \pi$, in terms of v_{ri}, $v_{\theta i}$, p_i and v_{ro}, $v_{\theta o}$, p_o for a range of the Reynolds numbers, characteristic viscosity ratio, volume fraction of the dispersed phase and the power-law index. Once the fully converged velocity and pressure fields are known, the individual and total drag coefficients can be evaluated as described below. The total drag coefficient is defined as:

$$C_d = \frac{2F_D}{\rho_o U_o^2 \pi R^2} \tag{13}$$

The pressure component C_{dp} is evaluated as:

$$C_{dp} = 2\int_0^\pi [p_o \sin 2\theta]_{r=1}\, d\theta \tag{14a}$$

and the frictional component C_{df} is evaluated as:

$$C_{df} = \frac{2^{(n_o+2)}}{Re_o}\int_0^\pi \left\{\eta_o\left[\left(\frac{\partial(v_\theta)_o}{\partial r} - \frac{(v_\theta)_o}{r}\right)\sin^2\theta - \left(\frac{\partial(v_r)_o}{\partial r}\right)\sin 2\theta\right]\right\}_{r=1} d\theta \tag{14b}$$

The total drag coefficient C_d is simply the sum of C_{dp} and C_{df}. The drag coefficient (or the sedimentation velocity) is expected to be a function of the Reynolds number, characteristic viscosity ratio, density ratio, power-law index and the concentration of the dispersed phase, and this relationship is developed in this work by seeking the numerical solutions to the governing equations.

4. Numerical methodology

Owing to the internal circulation, the motion of a drop in another immiscible fluid medium is different from that of a non-circulating bubble and of a solid particle. Therefore, one needs to solve the governing equations of both dispersed and continuous phases simultaneously which are coupled via the conditions requiring the continuity of the velocity and tangential stress at the interface. The governing Eqs. (1), (2a) and (2b) subject to the boundary conditions outlined in Eqs. (9)–(12) have been solved using a finite difference method based SMAC-implicit algorithm on a staggered grid arrangement. SMAC-implicit algorithm is a simplified version of the MAC method [50] which has been adapted here for power-law fluids. The application of an implicit algorithm on a staggered grid arrangement avoids the numerical instability commonly encountered at relatively low Reynolds numbers and shear-thinning fluids. Since the detailed descriptions of the numerical solver used in this work are available elsewhere [7,19], only the salient features are recapitulated here. For both phases, the diffusive and non-Newtonian terms have been discretized using the second order central difference scheme and the convective terms with the QUICK scheme [51]. The solution procedure is initiated at the centre of the drop ($r = 0$) until the drop surface ($r = 1$) is reached using the relevant boundary conditions for the inner fluid with the previous level value for $(v_\theta)_o$ assumed on the drop surface for the purpose of implementing the boundary conditions on the surface of the drop. In addition, the interfacial tangential velocity and pressure components on the surface of the drop resulting from the internal flow calculations have been used as boundary values for the outer fluid calculations for the same time-step. This sequence is continued until the continuity of the tangential velocity and the shear stress is satisfied within the prescribed level of tolerance and the so-called steady-state solution is obtained. The steady-state convergence criterion is fixed as, the maximum difference of any quantity between the two consecutive time-steps divided by Δt should fall below 10^{-3}, i.e.,

$$\frac{|z^{t+1} - z^t|}{\Delta t} \le 10^{-3} \tag{15}$$

In all cases, the approach to the convergence was asymptotic, although the number of time-steps required to achieve the steady-state is strongly dependent on the values of Re_o, n_o, k and Φ. However, for shear-thickening fluids ($n_o > 1$) convergence is faster than for shear-thinning fluids ($n_o < 1$) for same values of Re_o, k and Φ. Finally, the fully converged velocity and pressure fields were used to evaluate the derived quantities such as the individual and total drag coefficients, streamlines and vorticity contours, distributions of the viscosity, pressure, vorticity and tangential velocity on the surface of the drop, etc. The drag values, in turn, can be used to estimate the settling velocity of an ensemble of known characteristics.

4.1. Grid details

The boundary layer is expected to be thin at large Reynolds numbers and therefore, the grid needs to be sufficiently fine near the free surface. Furthermore, this problem becomes increasingly acute as the concentration of the dispersed phase is progressively reduced and the system approaches the single sphere limit [7]. Based on our previous study [7], it was found that a grid of size 60×70 (i.e., $3^\circ \times 0.025$ in angular and radial directions, respectively) was adequate to resolve the flow over the range of conditions as $1 \le Re_o \le 200$ and $0.1 \le k \le 50$. In this work, it is demonstrated that this grid can also be used when the continuous phase is a power-law medium. Three grids of sizes 45×70 (i.e., $4^\circ \times 0.025$), 60×70 (i.e., $3^\circ \times 0.025$) and 60×85 (i.e., $3^\circ \times 0.02$) have been used to simulate the results for $n_o = 0.6$ and $n_o = 1.6$, $\Phi = 0.2$ at $Re_o = 200$ and for $k = 0.1$ and 10, as shown in Table 1. Broadly speaking, differences in the values of the individual and total drag coefficient for any combination of the conditions are of the order of ±1–1.5%. For all values of the power-law index and the characteristic viscosity ratio, the difference between the drag values obtained with grids 45×70 and 60×70 is more than between that with grids 60×70 and 60×85. The improvement in the values of the total drag coefficient from the grid 60×85 compared to those by using grid 60×70 is negligible, but at an expense of significant increase in the CPU time. According to Roache [52], if the grid refinement ratio and the overall order of the scheme ≤2, then the relative difference is optimistic and conservative. Thus, a grid of size 60×70 has been used for all calculations reported in this study.

Table 1
Grid independence study for the power-law flow past an ensemble of dispersed phase concentration, $\Phi = 0.2$ at $Re_o = 200$

Grid size	$n_o = 0.6$			$n_o = 1.6$		
	C_{dp}	C_{df}	C_d	C_{dp}	C_{df}	C_d
$k = 0.1$						
45×70	0.1841	0.0852	0.2693	0.3259	0.4959	0.8218
60×70	0.1906	0.0880	0.2786	0.3307	0.4998	0.8305
60×85	0.1878	0.0862	0.2740	0.3269	0.4977	0.8246
$k = 10$						
45×70	0.7731	0.2619	1.0350	1.9900	1.9302	3.9202
60×70	0.7746	0.2631	1.0377	1.9920	1.9401	3.9321
60×85	0.7818	0.2645	1.0463	1.9780	1.9029	3.8809

5. Results and discussion

The scaling of the governing equations and of the boundary conditions suggests this flow to be governed by six dimensionless groups, namely, the Reynolds number (Re_o), concentration of the dispersed phase (Φ), characteristic viscosity ratio (k), density ratio (λ), power-law index (n_o) and drag coefficient (C_d). In this study, the roles of all these parameters are studied, except that of the density ratio (λ). Following the recent works of Juncu [53] and of Feng and Michaelides [54] who found that the drag coefficient values of a fluid sphere to be virtually independent of the density ratio over the range of $0.1 \leq \lambda \leq 10$, thus, this ratio was set equal to unity in this work. Further, in this study, extensive numerical results have been presented over the following ranges of parameters: $1 \leq Re_o \leq 200$, $0.2 \leq \Phi \leq 0.6$, $0.1 \leq k \leq 50$ and $0.6 \leq n_o \leq 1.6$.

5.1. Validation of results

Before presenting the new results for power-law fluids, it is desirable to ascertain the accuracy and reliability of the numerical results obtained in this work. This is accomplished by comparing the present results with the previously available reliable values of the drag coefficients available in the literature. Since the numerical solver used here has been extensively validated for the limiting cases of the flow of Newtonian fluids past isolated bubbles, drops and solid particles and in ensembles of droplets elsewhere [7,19], only the additional comparisons are shown for the case of slow motion ($Re_o = 1$) of ensembles of Newtonian fluid spheres in power-law liquids with the approximate results of Jarzebski and Malinowski [40] (Table 2). For all values of the viscosity ratio and the power-law index, the two values are seen to be within ±5% of each other. Broadly speaking, the two values deviate increasingly as the degree of shear-thinning increases. This is not at all surprising since the upper and lower bounds diverge with the increasing degree of shear-thinning behaviour. Furthermore, differences of this magnitude are not at all uncommon in such numerical studies due to the differences stemming from grid errors, solution procedure, etc. [52]. In view of these factors and based on our previous experience [7,19], the present results are believed to be reliable and accurate to within ±2–4%.

Table 2
Comparison of the present values of C_d for the slow motion ($Re_o = 1$) of Newtonian and shear-thinning liquids

Hold-up (Φ)	Power-law index (n_o)	Total drag coefficient (C_d)	
		Jarzebski and Malinowski [40]	Present
$k = 0.1$			
0.2	1	42.96	42.1083
	0.8	33.24	33.1104
	0.6	25.68	26.3009
0.4	1	72.00	69.8154
	0.8	49.80	48.4403
	0.6	34.68	33.9967
$k = 10$			
0.2	1	118.56	122.4372
	0.8	84.6	84.7666
	0.6	59.4	58.3511
0.4	1	354.0	369.7882
	0.8	215.64	208.9723
	0.6	125.64	117.5646

5.2. Flow patterns

The translation of a fluid sphere is different from that of a solid sphere due to the internal circulation within the drop, which is strongly influenced by the viscosity ratio, k. Therefore, owing to the finite angular velocity on the surface of the drop, the point of separation is the point at which this velocity becomes zero. Currently available results show that there will be no recirculation for any value of the Reynolds number for $k \leq 1$ for Newtonian [7,53,54] and in power-law fluids [19] provided the drop retains its spherical shape. Similarly, no such return-flow occurs for the case of Reynolds number up to $Re_o \leq 20$ for any value of the viscosity ratio and power-law index.

Fig. 2 shows the effect of the viscosity ratio, k, on the streamlines (upper half) and the iso-vorticity (lower half) contours for the case of a shear-thinning ($n_o = 0.6$) fluid past an ensemble of $\Phi = 0.2$ at $Re_o = 200$. From Fig. 2(a), it can be seen that for $k = 0.1$, both streamlines and vorticity contours inside and outside the drop are symmetric and this trend continues for streamlines up to $k = 1$, but the vorticity contours begin to show asymmetry due to the increasing amount of vorticity being transmitted to the interior of the drop. With a further increase in the value of the viscosity ratio, $k > 1$, the centre of the inside circulation also starts to move towards the front stagnation point.

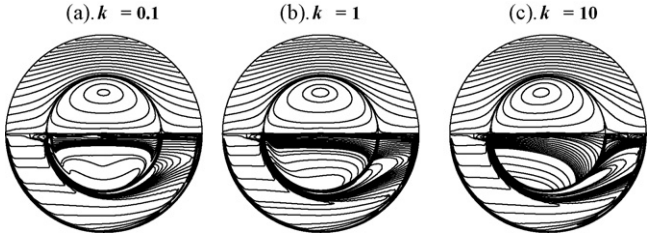

Fig. 2. Effect of k on streamlines and iso-vorticity contours of an ensemble of $\Phi = 0.2$ at $Re_o = 200$ and $n_o = 0.6$.

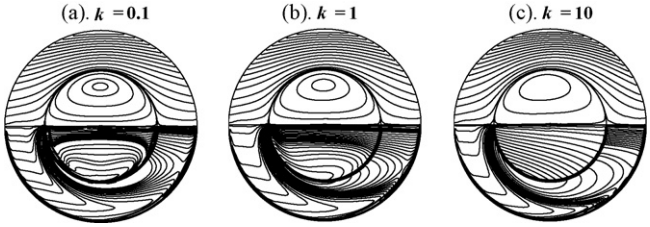

Fig. 3. Effect of k on streamlines and iso-vorticity contours of an ensemble of $\Phi = 0.2$ at $Re_o = 200$ and $n_o = 1.6$.

This is so in part due to the large amount of vorticity is being created on the surface of the drop which has to be to accommodated inside the drop. Fig. 3 shows the effect of the viscosity ratio on the streamlines and iso-vorticity contours for the case of a shear-thickening ($n_o = 1.6$) fluid for $\Phi = 0.2$ at $Re_o = 200$. Qualitatively similar trends of the streamlines and vorticity patterns have been observed for the other values of the Reynolds number, power-law index, characteristic viscosity ratio and the drop hold-up, hence these are not shown here. Furthermore, it is worthwhile to add here that for $k \ll 1$, the inner Reynolds number would be large and this could lead to asymmetry and instability of the flow within the droplet. However, since the minimum value of k in the present study is only 0.1, this phenomenon was not observed here. On the other hand, this could easily occur in bubbles leading to significant deviations from symmetric flow conditions.

Further examination of the detailed pressure coefficient, effective viscosity and tangential velocity on the surface of a representative drop revealed these to be similar as that for Newtonian systems [7] and hence these are not repeated here. However, the key points are summarized here. Broadly, for fixed values of the Reynolds number and the concentration of the dispersed phase, the surface pressure coefficient in the front half of the drop is almost independent of the value of the power-law index, particularly for $k \leq 1$. In contrast, in the rear half of the drop surface, a definitive influence of n_o is seen depending on the value of k. As the value of k is increased, the effect of n_o on surface pressure coefficient in the rear half of the drop becomes significant. For the case of shear-thinning fluids ($n_o < 1$), the recovery of pressure in the rear end of the drop is larger than in the case of Newtonian fluid. Thus, C_{dp} is smaller for shear-thinning fluids than that in the case of Newtonian fluids; for the case of shear-thickening fluids ($n_o > 1$), an opposite trend is observed. Similarly, the effect of the power-law index on the tangential velocity is more significant for large values of the characteristic viscosity ratio irrespective of the values of the Reynolds number and the concentration of the dispersed phase. Thus, for instance, for all values of Re_o, k and Φ, the value of the tangential velocity is larger in shear-thinning fluids than in the case of Newtonian fluid. For shear-thickening fluids ($n_o > 1$), an opposite trend has been observed.

5.3. Drag phenomena

Fig. 4 shows the effect of the power-law index on the total drag coefficient as a function of the Reynolds number for $\Phi = 0.2$ for different values of k. For all values of k and n_o, the typical behaviour of C_d–Re_o is qualitatively similar, i.e., as the value of the Reynolds number increases, the total drag coefficient decreases. For a fixed value of the characteristic viscosity ratio and the Reynolds number, as the value of the power-law index increases, the drag coefficient increases. The shear-thinning behaviour is seen to reduce the drag below its Newtonian value whereas shear-thickening is seen to augment it. For fixed values of the power-law index and the Reynolds number, as the value of the characteristic viscosity ratio increases, the drag coefficient increases due to the suppression of the internal circulation. Qualitatively similar trends have been observed for the other values of the volume fraction of the dispersed phase. Fig. 5 shows the effect of the concentration of the dispersed phase on the total drag coefficient for a shear-thinning fluid, $n_o = 0.6$ (a–c) and a shear-thickening fluid, $n_o = 1.6$ (d–f) for different values of k. For both values of n_o, although, for all values of k and any fixed value of Re_o, as the value of Φ increases, the value of C_d increases, but the effect of Φ is more significant for large values of k, i.e., going towards the solid-like particles. Fig. 6 shows the effect of the characteristic viscosity ratio on C_d as a function of Re_o for a shear-thinning fluid, $n_o = 0.6$ (a–c) and a shear-thickening fluid, $n_o = 1.6$ (d–f) for different values of Φ. Irrespective of the

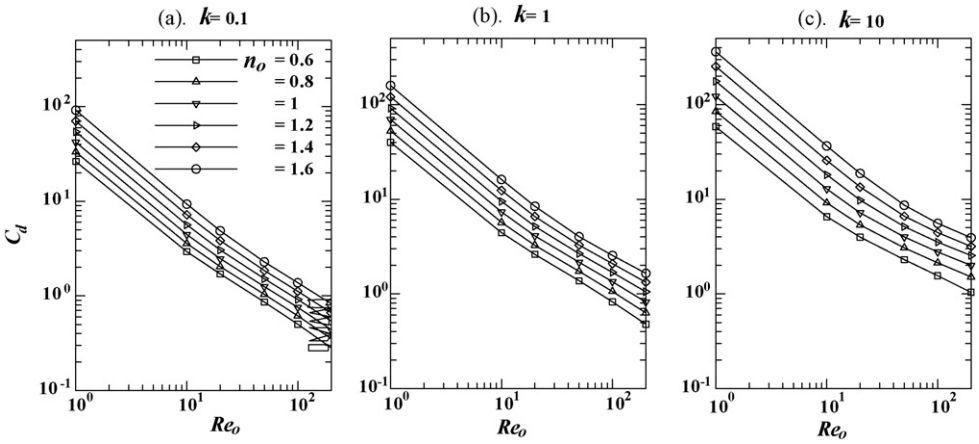

Fig. 4. Effect of n_o on C_d as a function of Re_o for an ensemble of $\Phi = 0.2$ for different values of k.

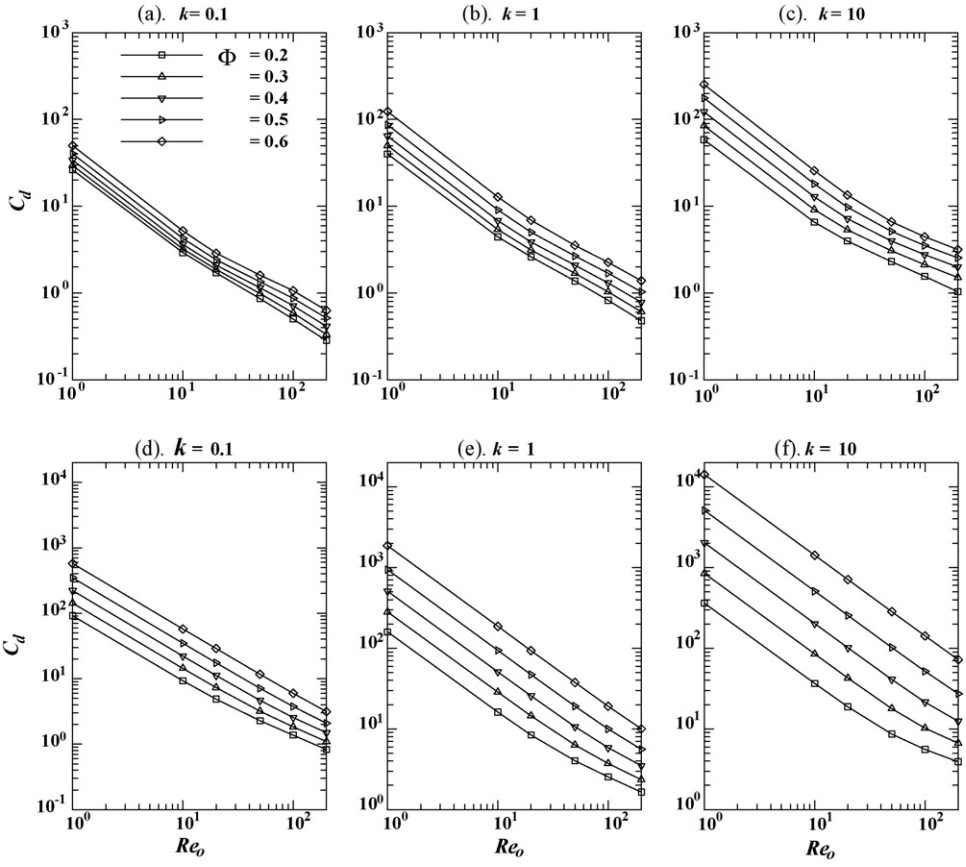

Fig. 5. Effect of Φ on C_d as a function of Re_o when $n_o = 0.6$ (a–c) and $n_o = 1.6$ (d–f) for different values of k.

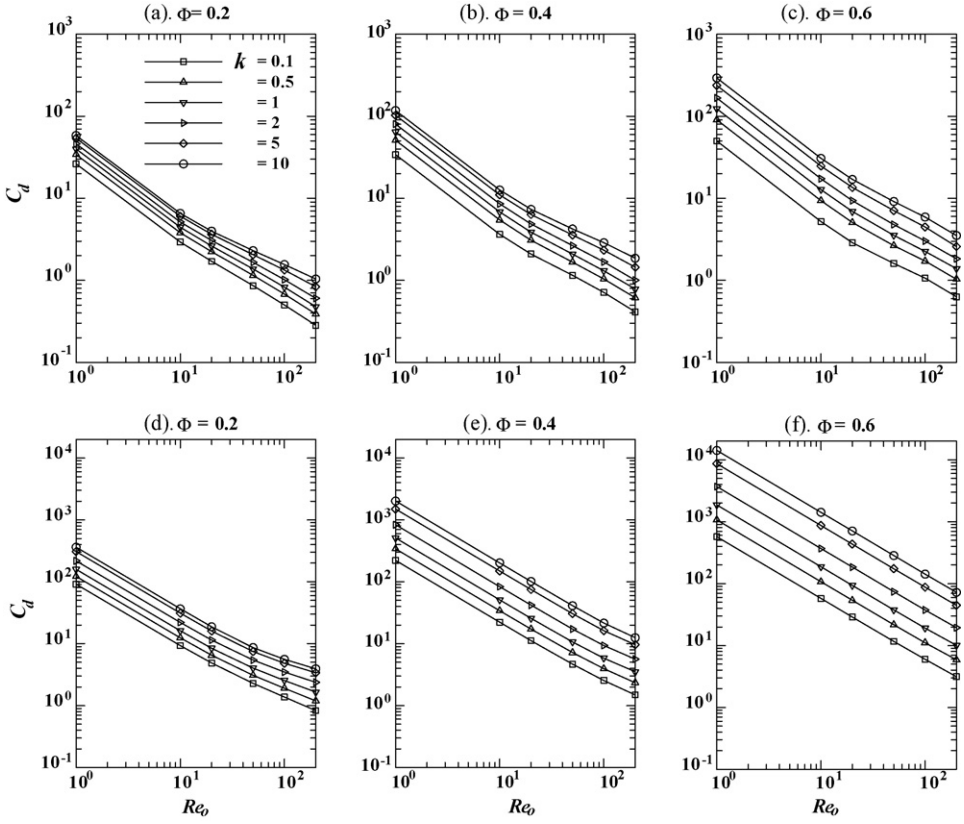

Fig. 6. Effect of k on C_d as a function of Re_o when $n_o = 0.6$ (a–c) and $n_o = 1.6$ (d–f) for different values of Φ.

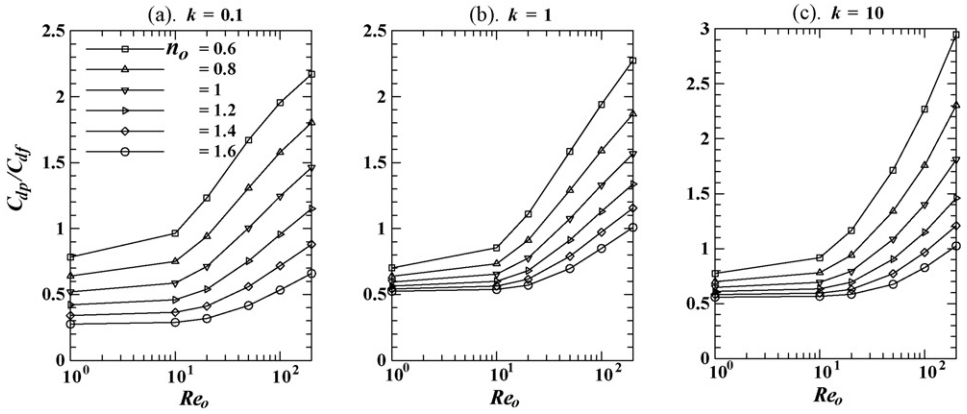

Fig. 7. Effect of n_o on C_{dp}/C_{df} as a function of Re_o for an ensemble of $\Phi = 0.2$ for different values of k.

nature of fluid, for all values of Φ and Re_o, as the value of the characteristic viscosity ratio increases, the value of C_d increases, though the effect of the characteristic viscosity ratio is seen to be more significant for large values of Φ.

In order to delineate the relative contributions of the individual drag coefficients, the present results have been further analyzed in terms of the ratio (C_{dp}/C_{df}). Fig. 7 shows the variation of this ratio with the power-law index for $\Phi = 0.2$ for different values of k. For all values of k and of n_o, the effect of Re_o on (C_{dp}/C_{df}) is modest up to about $Re_o \leq 20$, thereby suggesting that both viscous and pressure forces rise more or less at the same rate. Beyond this value of the Reynolds number, this ratio increases thereby suggesting poor pressure recovery in the rear of the drop. For all values of k and of Re_o, as the value of n_o increases the value of (C_{dp}/C_{df}) decreases; however, this dependence weakens with the increasing value of k. Qualitatively similar trends have been observed for other values of the volume fraction of the dispersed phase. Fig. 8 shows the effect of the volume fraction of the dispersed phase on (C_{dp}/C_{df}) for a range of values of Re_o for a shear-thinning fluid, $n_o = 0.6$ (a–c) and for a shear-thickening fluid, $n_o = 1.6$ (d–f) for different values of k. For $k = 0.1$, the effect of Φ is negligible up to

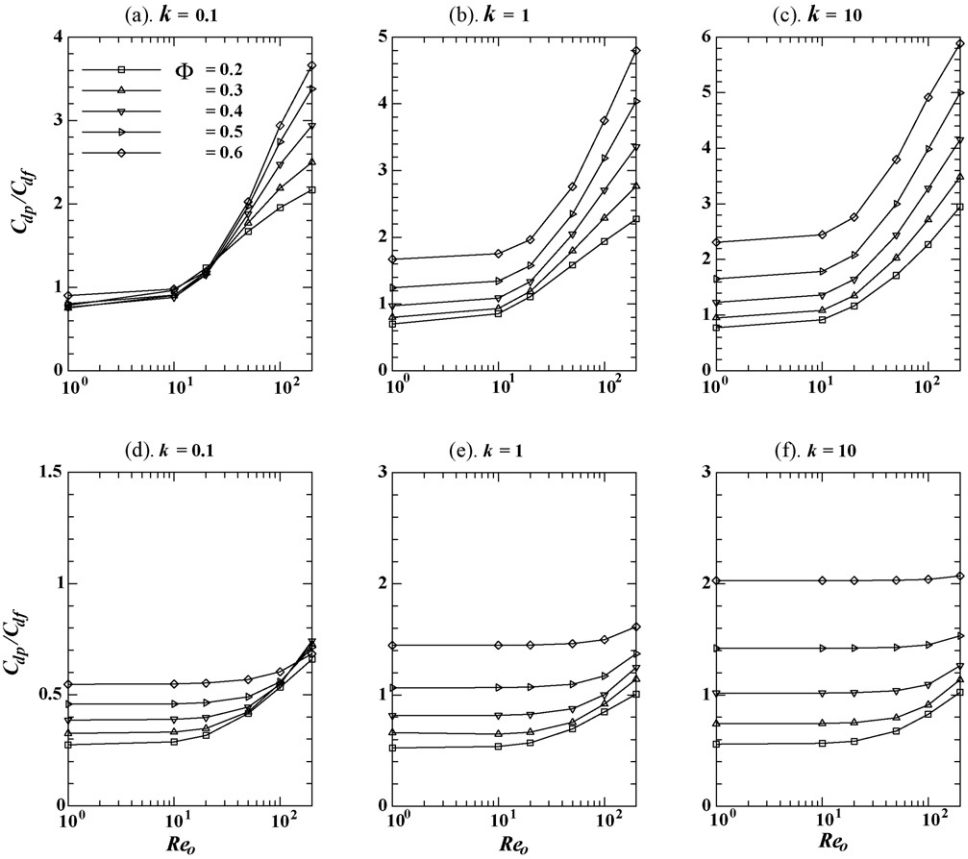

Fig. 8. Effect of Φ on C_{dp}/C_{df} as a function of Re_o when $n_o = 0.6$ (a–c) and $n_o = 1.6$ (d–f) for different values of k.

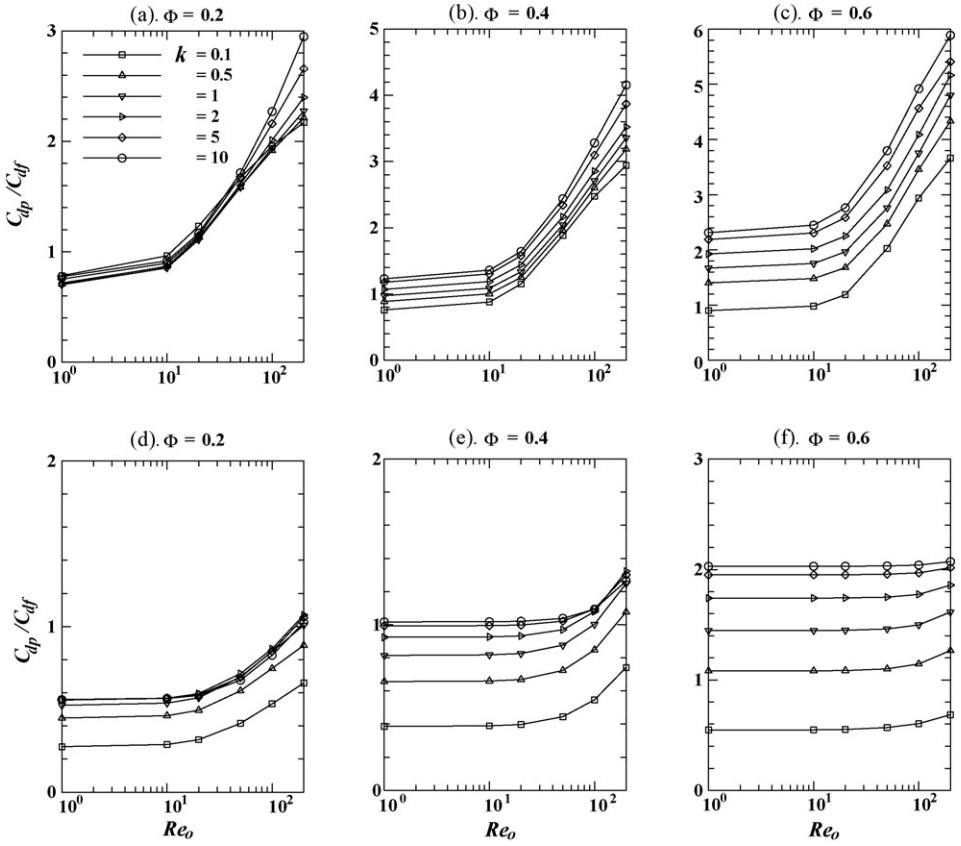

Fig. 9. Effect of k on C_{dp}/C_{df} as a function of Re_o when $n_o = 0.6$ (a–c) and $n_o = 1.6$ (d–f) for different values of Φ.

$Re_o < 50$ in the case of shear-thinning fluids, whereas it is negligible for $Re_o > 50$ in the case of shear-thickening fluids. However, as the value of k is gradually increased, the effect of Φ becomes dominant for both shear-thinning and shear-thickening fluids. For shear-thickening fluids, the effect of Re_o on the value of (C_{dp}/C_{df}) becomes negligible for large values of Φ when $k \geq 2$. Fig. 9 shows the effect of the characteristic viscosity ratio on the value of (C_{dp}/C_{df}) as a function of Re_o for a shear-thinning fluid, $n_o = 0.6$ (a–c) and for a shear-thickening fluid, $n_o = 1.6$ (d–f) for different values of Φ. For shear-thinning fluids, the effect of k on (C_{dp}/C_{df}) is very small for small values of Φ; however, it increases progressively as the value of Φ increases. For shear-thickening fluids, as the value of Φ increases, (C_{dp}/C_{df})–Re_o profile becomes flat for all values of k. Furthermore, it will be useful to delineate the critical values of the Reynolds number at which the ratio (C_{dp}/C_{df}) is approximately one and it is observed that for fixed values of k, the critical value of the Reynolds number increases as the value of n_o and/or Φ increases. Broadly, this ratio is constant at low Reynolds numbers (up to about ~10–20 and then begins to increase). In shear-thickening fluids, it seems to stay constant up to somewhat larger values of the Reynolds numbers than that in shear-thinning fluids otherwise under identical conditions. Clearly, the exact transitional values of the Reynolds number are determined by an intricate interplay between the severity of the shear-thinning or shear-thickening fluid behaviour and the inter-drop separation, i.e., the value of Φ.

Finally, from an engineering application standpoint, it is useful to develop a predictive correlation based on the present numerical results which can be used to estimate the sedimentation velocity of ensembles of mono-size Newtonian fluid spheres in power-law liquids. As far as known to us, there is no such prior correlation available in the literature embracing such wide ranging conditions. The following form was found to be satisfactory to correlate the present numerical results:

$$C_d = C_{d,o}\left\{1 + 0.012(1-\Phi)^{3n_o-2} Re_o^{0.92} k^{0.19}\right\} \tag{16}$$

where $C_{d,o}$ is given by

$$C_{d,o} = \left(\frac{2^{(2n_o+1)}}{Re_o}\right)\left\{\frac{2\left(1-\Phi^{(3n_o+2)/(2n_o+1)}\right) + \left[(n_o+2)/(n_o+1) + 2\Phi^{(3n_o+2)/(2n_o+1)}\right]k}{\left(1-\Phi^{n_o/(4n_o-1)}\right)\left(1-\Phi^{(3n_o+2)/(2n_o+1)}\right) + \left[1-(3/2)\Phi^{n_o/(4n_o-1)} + (3/2)\Phi^{(3n_o+2)/(2n_o+1)} - \Phi^2\right]k}\right\} \tag{17}$$

For $n_o = 1$ and $Re_o \to 0$, Eq. (17) reduces to the analytical solution of Gal-Or and Waslo [39]. Eq. (16) reproduces the present numerical results (1370 data points) with an average error of ±13.4% which rises to maximum of ±57.5%. However, if the results for $Re_o = 1$ relating to shear-thickening fluids are excluded, the average and maximum errors are reduced to ±10 and ±40%, respectively. For the limiting condition of $n_o = 1$, Eq. (16) reduces to our expression for a Newtonian continuous phase

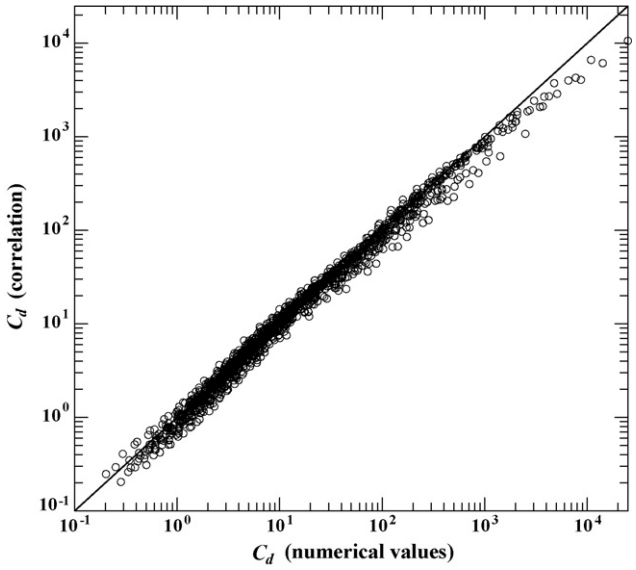

Fig. 10. Comparison of the present numerical values of C_d with those obtained by using the proposed correlation.

[7]. Furthermore, admittedly it would be desirable to include the limiting cases of $k = 0$ (bubbles) and $k = \infty$ (solid spheres) in Eq. (16), but unfortunately, due to the paucity of results in the ranges of $0 \leq k \leq 0.1$ and $50 \leq k \leq \infty$, it is proved impossible to accomplish this goal with acceptable levels of accuracy. However, Eq. (16) can be used to estimate the drag for extreme values of the characteristic viscosity ratio, i.e., for $k = 0$ and $k = \infty$ in the range of $0.6 \leq n \leq 1.6$ for the creeping flow conditions. On the other hand, reliable correlations are already available in the literature for the cases of swarms of bubbles [23,24] and assemblages of solid spheres [33] in power-law liquids in the intermediate range of Reynolds numbers. Finally, it is appropriate to add here that the present results in these limits ($k = 0$ and $k = \infty$) are consistent with the literature values [7,19]. Fig. 10 shows the parity plot of the numerical and predicted results using Eq. (16).

In summary, it is appropriate to reiterate here that though the present results are based on an idealized cell model which does not take into account the effects arising from the collisions, drop deformation, coalescence, etc. which inevitably occur in moderate to concentrated systems. In spite of these limitations, Eq. (16) does offer an useful first order approximation for the estimation of the rate of sedimentation of ensembles of droplets in quiescent power-law liquids simply from a knowledge of the pertinent variables like drop size, concentration of the dispersed phase, density and power-law constants of the two phases. Of course, the future studies will try to address the issues of collisions, shape changes, etc.

6. Conclusions

In this work, numerical predictions of drag on ensembles of fluid spheres sedimenting in power-law fluids have been used to delineate their dependence on the Reynolds number, power-law index, characteristic viscosity ratio and the volume fraction of the dispersed phase. For fixed values of the characteristic viscosity ratio and the Reynolds number, the total drag coefficient in a shear-thinning fluid is reduced below its Newtonian value whereas it is augmented in shear-thickening fluids. For fixed values of the power-law index and Reynolds number, as the value of the characteristic viscosity ratio increases, the drag coefficient also increases due to the reduced level of internal circulation. Though, for all values of k and of Re_o, as the value Φ increases, the value of C_d increases, this effect is more significant for large values of k which is again due to the decreasing level of circulation. For shear-thinning fluids, the effect of Φ on (C_{dp}/C_{df}) is negligible up to $Re_o = 50$ for the value of $k = 0.1$. For shear-thinning fluids ($n_o < 1$), the effect of k on (C_{dp}/C_{df}) is very weak for small values of Φ which becomes progressively more significant as the value of Φ increases. On the other hand, for shear-thickening fluids ($n_o > 1$), the effect of Re_o on (C_{dp}/C_{df}) is negligible for $Re_o > 50$ for $k = 0.1$, whereas, for $k \geq 2$, the effect of Re_o on the value of (C_{dp}/C_{df}) becomes negligible for large values of Φ. For small values of Φ, the effect of k is negligible on (C_{dp}/C_{df}) for any value of Re_o. For any combination of the values of Re_o, k, n_o and Φ in the range studied herein, no flow separation was observed. A simple predictive expression is developed which can be used to estimate the settling velocity of an ensemble of uniform size droplets in clean power-law fluids.

References

[1] W.D. Deckwer, Bubble Column Reactors, Wiley, New York, 1992.
[2] P.J. Fryer, D.L. Pyle, C.D. Reilly, Chemical Engineering for the Food Industry, Blackie Academic and Professional, London, U.K, 1997, pp. 400–431.
[3] L. Schramm, Emulsions, Foams and Suspensions, Wiley-VCH, New York, 2005.
[4] R.P. Chhabra, Bubbles, Drops, and Particles in Non-Newtonian Fluids, second ed., CRC Press, Boca Raton, FL, USA, 2006, pp. 1–5.
[5] R. Clift, J.R. Grace, M.E. Weber, Bubbles, Drops and Particles, Academic press, New York, USA, 1978, pp. 30–46, 125–137.
[6] E.E. Michaelides, Particles, Bubbles and Drops: Their Motion, Heat and Mass Transfer, World Scientific, Singapore, 2006, pp. 23–156.
[7] N. Kishore, R.P. Chhabra, V. Eswaran, Chem. Eng. Res. Des. 84 (2006) 1180–1193.
[8] R.P. Chhabra, J.F. Richardson, Non-Newtonian Flow in the Process Industries, Butterworth-Heinemann, Oxford, UK, 1999, pp. 33–34.
[9] D.G. Karamanev, K. Dewsbury, A. Margaritis, Chem. Eng. Sci. 60 (2005) 4655–4657.
[10] D. Rodrigue, Can. J. Chem. Eng. 80 (2002) 289–292.
[11] M. Dziubinski, M. Orczykowska, P. Budzynski, Chem. Eng. Sci. 58 (2003) 2441–2443.
[12] A.A. Kulkarni, J.B. Joshi, Ind. Eng. Chem. Res. 44 (2005) 5873–5931.
[13] S.D. Dhole, R.P. Chhabra, V. Eswaran, Ind. Eng. Chem. Res. 46 (2007) 939–946.
[14] D.I. Graham, T.E.R. Jones, J. Non-Newtonian Fluid Mech. 54 (1994) 465–488.
[15] S.D. Dhole, R.P. Chhabra, V. Eswaran, Ind. Eng. Chem. Res. 45 (2006) 4773–4781.
[16] T. Gurkan, Chem. Eng. Commun. 80 (1989) 53–67.
[17] R.P. Chhabra, J. Bangun, Can. J. Chem. Eng. 75 (1997) 817–822.
[18] D. Rodrigue, J.F. Blanchet, Proceedings of the Fourth International Conference on Multiphase Flows (ICMF-2001), New Orleans, LA, 2001 (paper #933).
[19] N. Kishore, R.P. Chhabra, V. Eswaran, Chem. Eng. Sci. 62 (2007) 2422–2434.
[20] M. Ohta, E. Iwasaki, E. Obata, Y. Yoshida, J. Non-Newtonian Fluid Mech. 132 (2005) 100–107.
[21] S. Gummalam, R.P. Chhabra, Can. J. Chem. Eng. 65 (1987) 1004–1008.

[22] S. Gummalam, K.A. Narayan, R.P. Chhabra, Int. J. Multiphase Flow 14 (1988) 361–371.
[23] M. Manjunath, R.P. Chhabra, Int. J. Eng. Sci. 30 (1992) 871–878.
[24] M. Manjunath, A. Tripathi, R.P. Chhabra, T. Sundararajan, Int. J. Eng. Sci. 32 (1994) 927–933.
[25] R.P. Chhabra, Can. J. Chem. Eng. 76 (1998) 137–140.
[26] J. Happel, AIChE J. 4 (1958) 197–201.
[27] S. Kuwabara, J. Phys. Soc. Jpn. 14 (1959) 524–532.
[28] J. Zhu, Chem. Eng. Sci. 56 (2001) 2237–2241.
[29] G. Marrucci, Ind. Eng. Chem. Fundam. 4 (1965) 224–225.
[30] K.W. Lee, L.D. Reed, C.H. Jung, J. Environ. Eng. 125 (1999) 634–637.
[31] Y. Kawase, J.J. Ulbrecht, Chem. Eng. Sci. 36 (1981) 1193–1202.
[32] Y. Kawase, J.J. Ulbrecht, Chem. Eng. Commun. 8 (1981) 233–249.
[33] S.D. Dhole, R.P. Chhabra, V. Eswaran, Chem. Eng. Res. Des. 82 (2004) 642–652.
[34] R. Shukla, S.D. Dhole, R.P. Chhabra, V. Eswaran, Chem. Eng. Sci. 59 (2004) 645–659.
[35] R.P. Chhabra, J. Comiti, I. Machac, Chem. Eng. Sci. 56 (2001) 1–27.
[36] D. Ciceron, J. Comiti, R.P. Chhabra, M. Renaud, Chem. Eng. Sci. 57 (2002) 3225–3234.
[37] J.P. Hsu, E. Lee, Y. Huang, Langmuir 20 (2004) 2149–2156.
[38] E. Lee, C. Tai, J.P. Hsu, C. Chen, Langmuir 20 (2004) 7952–7959.
[39] B. Gal-Or, S. Waslo, Chem. Eng. Sci. 23 (1968) 1431–1446.
[40] A.B. Jarzebski, J.J. Malinowski, Chem. Eng. Sci. 41 (1986) 2569–2573.
[41] A.B. Jarzebski, J.J. Malinowski, Chem. Eng. Commun. 49 (1987) 235–246.
[42] A.B. Jarzebski, J.J. Malinowski, Can. J. Chem. Eng. 65 (1987) 680–684.
[43] J. Zhu, W. Deng, Chem. Eng. Sci. 49 (1994) 147–150.
[44] J. Zhu, Int. J. Multiphase Flow 21 (1995) 935–940.
[45] A. Tripathi, R.P. Chhabra, Int. J. Eng. Sci. 32 (1994) 791–803.
[46] J.M. Ferreira, A.A. Soares, R.P. Chhabra, Fluid Dyn. Res. 32 (2003) 201–215.
[47] D. Prasad, K.A. Narayan, R.P. Chhabra, Int. J. Eng. Sci. 28 (1990) 215–230.
[48] C.H. Jung, K.W. Lee, Environ. Eng. Sci. 24 (2007) 216–227.
[49] R.B. Bird, W.E. Stewart, E.N. Lightfoot, Transport Phenomena, second ed., John Wiley, New York, 2002, pp. 240–241, 844.
[50] F.H. Harlow, J.E. Welch, Phys. Fluids 8 (1965) 2182–2188.
[51] B.P. Leonard, Comp. Methods Appl. Mech. Eng. 19 (1979) 59–98.
[52] P.J. Roache, Trans. ASME, J. Fluids Eng. 116 (1994) 405–413.
[53] G. Juncu, Int. J. Heat & Fluid Flow 20 (1999) 414–421.
[54] Z.G. Feng, E.E. Michaelides, Trans. ASME J. Fluids Eng. 123 (2001) 841–849.